Available online at www.sciencedirect.com

ScienceDirect

www.elsevier.com/locate/brainres

Brain Research

Research Report

Responses of single neurons and neuronal ensembles in frog first- and second-order olfactory neurons

Jean-Pierre Rospars[a,*], Pavel Sanda[c], Petr Lansky[c], Patricia Duchamp-Viret[b]

[a]UMR 1272 Physiologie de l'Insecte: Signalisation et Communication & Unité Mathématiques et Informatique Appliquées, INRA, F-78000 Versailles, France

[b]Centre de Recherche en Neurosciences Lyon, INSERM U1028/CNRS UMR 5292, 50 Avenue Tony Garnier, F-69366 Lyon Cedex, France

[c]Institute of Physiology, Academy of Sciences of the Czech Republic, Videnska 1083, CZ-142 20 Prague 4, Czech Republic

ARTICLE INFO

Article history:
Accepted 8 May 2013
Available online 18 May 2013

Keywords:
Olfactory receptor neuron
Mitral cell
Dose–response curve
Intensity coding
Population coding

ABSTRACT

A major challenge in sensory neuroscience is to elucidate the coding and processing of stimulus representations in successive populations of neurons. Here we recorded the spiking activity of receptor neurons (RNs) and mitral/tufted cells (MCs) in the frog olfactory epithelium and olfactory bulb respectively, in response to four odorants applied at precisely controlled concentrations. We compared how RN responses are translated in MCs. We examined the time course of the instantaneous firing frequency before and after stimulation in neuron ensembles and the dependency on odorant concentration of the number of action potentials fired in a preselected 5-s time window (dose–response curves) in both single neurons and neuron ensembles. In RNs and MCs, the dose–response curves typically increase then decrease and are well described by alpha functions. We established the main quantitative properties of these curves, including the distributions of concentrations at threshold and maximum responses. We showed that the main transformations occurring in the transition from RNs to MCs is the lowering of the firing threshold and a large decrease in the total number of spikes fired. We also found that the number of action potentials fired by recorded neurons and hence their energy consumption is independent of odorant concentration, and that this is a consequence of their time- and concentration-dependent activities.

This article is part of a Special Issue entitled Neural Coding 2012.

1. Introduction

In the olfactory system, odor stimuli are detected by different odorant receptors (ORs) borne by thousands first-order neurons (olfactory receptor neurons RNs) that send signals to fewer second-order neurons—mitral cells (MCs) in the vertebrate olfactory bulb and projection neurons (PNs) in the insect antennal lobe; in the bulb/lobe the olfactory information is processed by a complex neural network involving local and centrifugal neurons (Buck, 1996; Rospars, 1988; Shepherd et al., 2004). To elucidate how the olfactory signal message conveyed by RNs is transformed in the

*Corresponding author. Fax +33 1 30 83 31 19.
E-mail address: jean-pierre.rospars@versailles.inra.fr (J.-P. Rospars).

0006-8993/$ - see front matter © 2013 Elsevier B.V. All rights reserved.
http://dx.doi.org/10.1016/j.brainres.2013.05.018

output carried by MCs/PNs is essential for a proper understanding of olfactory processing and the properties of odor perception (Duchamp-Viret et al., 2003; Chaput et al., 2012). Moreover, this transformation is likely representative of the strategy used in cortical preprocessing (Niessing and Friedrich, 2010).

All early sensory systems possess four basic properties. First, single sensory neurons fire action potential at a rate that increases with stimulus intensity (Adrian, 1950). Second, they best process their natural stimuli that occur most frequently (efficient coding; Laughlin, 1981; Simoncelli and Olshausen, 2001). In particular, the latter property predicts the first one and indicates that the sigmoid response curve to a stimulus reflects the cumulative distribution of its intensities in nature. Third, energy consumption is a strong constraint because neural processing is metabolically expensive (Levy and Baxter, 1996; Lennie, 2003; Niven and Laughlin, 2008), which might favor codes using as few spikes as possible (Barlow, 1969; Olshausen and Field, 2004). Fourth, any specific feature of the world is encoded in the concerted activity of many neurons so that neural coding can be fully understood only at the neuron population level (Pouget et al., 2003; Kass et al., 2005).

The olfactory system clearly possesses the first and last properties. The successive neural layers of the system display population coding (Friedrich and Stopfer, 2001; Ito et al., 2009; Laurent, 2002; Lledo and Lagier, 2006; Shepherd et al., 2004; Wilson and Mainen, 2006) and each ORN obeys Adrian's law in a specific manner. It is known that the responses to monomolecular odors across RNs are highly variable in threshold, dynamic range and maximum rate (de Bruyne et al., 2001; Ito et al., 2009; Münch et al., 2013; Rospars et al., 2003, 2008), even in ORNs expressing the same OR (Grosmaître et al., 2006). Is it also true for MCs? To address this question, we compared the properties of single RNs and MCs in response to stimulations differing in quality (across four odorants) and intensity (across odorant concentrations varying over six orders of magnitudes). We examined two complementary features: the firing rate of individual neurons in order to describe the time course of the responses and the number of spikes fired during a specified time (2 s) to analyze their dependency on stimulus concentration. We found that both RNs and MCs obey the same quantitative rules in their average responses and their variability. The MCs fire less odorant-evoked spikes but more spontaneous spikes than RNs. Although their dynamic ranges are similar in width, the thresholds of MCs are shifted toward lower concentration with respects to those of RNs. Like in RNs, all response properties (maximum number of spikes fired, threshold, dynamic range) of MCs are extremely variable so that both display the "page-filling" property previously described for RNs (Rospars et al., 2003).

However, the status of the other two properties is less clear. Studies of efficient olfactory coding in insects, whose olfactory system has the same functional architecture as in vertebrates (Hildebrand and Shepherd, 1997), concluded that ORNs are relatively inefficient at quality coding (Abbott and Luo, 2007; Bhandawat et al., 2007) and efficient at intensity coding (Kostal et al., 2008). Energy consumption has been modeled in mammalian glomeruli (Nawroth et al., 2007) but not at the population level, so the problem of global energy consumption remains open. In particular, it is not known to what extent the four properties are compatible with one another. The first two properties seem in good agreement. In conjunction with the fourth one, they lead to predict that a neuron population should fire more spikes for strong than for weak stimuli. However, this may conflict with the third (spike saving) property. To address this issue we investigated the global properties of ensembles of RNs and MCs. We found that the number of action potentials encoding the same olfactory information in such ensembles is considerably smaller in MCs than in RNs in accordance with Barlow's (1969) prediction. We found also that, in both ensembles stimulated at various concentrations, the maximum rate and the total number of spikes fired in a long enough time period (2 s or more) are nearly constant, independent of odorant concentration. We show that this a priori surprising concentration-independence, previously observed also in insects (Stopfer et al., 2003), does not contradict Adrian's law for single neurons. However, we suggest that it is a property of the ensemble of recorded neurons and not of the whole system. Actually, the number of active neurons and consequently the total activity are expected to increase with concentration which solves an apparent paradox.

2. Results

The unit activity of two connected populations of neurons, receptor neurons (RNs) of the ventral olfactory epithelium and mitral cells (MCs) of the olfactory bulb, were studied before and after stimulation with four odorants (anisole, camphor, isoamyl acetate and limonene) on the whole range of concentrations to which these neurons were sensitive (Fig. 1). The number of records retained in each category were 550 (RNs) and 785 (MCs) with similar number of records per odorant in the range 276–311 (Table 2). In the first section, the time-evolution of the overall firing rate is examined before, during and after stimulation. In the second section, the effects of odorant concentration are analyzed across neurons at the single-cell level; whereas, in the third section it is analyzed on pooled neurons across concentrations.

2.1. *Time dependency of the firing rates in neuron ensembles*

We investigated first the time-dependency of neural activity. To this end, the instantaneous firing rates were estimated by convolving the spikes with a Gaussian kernel before and after stimulation with all odorants and concentrations pooled together (Fig. 2A).

Before stimulation, the activity was constant in both RNs and MCs. The spontaneous firing rate during the 30 s preceding the stimulus, determined as the total number of action potentials (APs) divided by the duration of spontaneous activity, was significantly lower in RNs (0.45 AP/s) than in MC neurons (0.55 AP/s). As shown by *t*-test, RNs and MCs were significantly different ($p<0.001$). Cumulative spike counts (Fig. 2B) confirmed the stationarity of spontaneous activity and its lower rate in RNs, which is more apparent

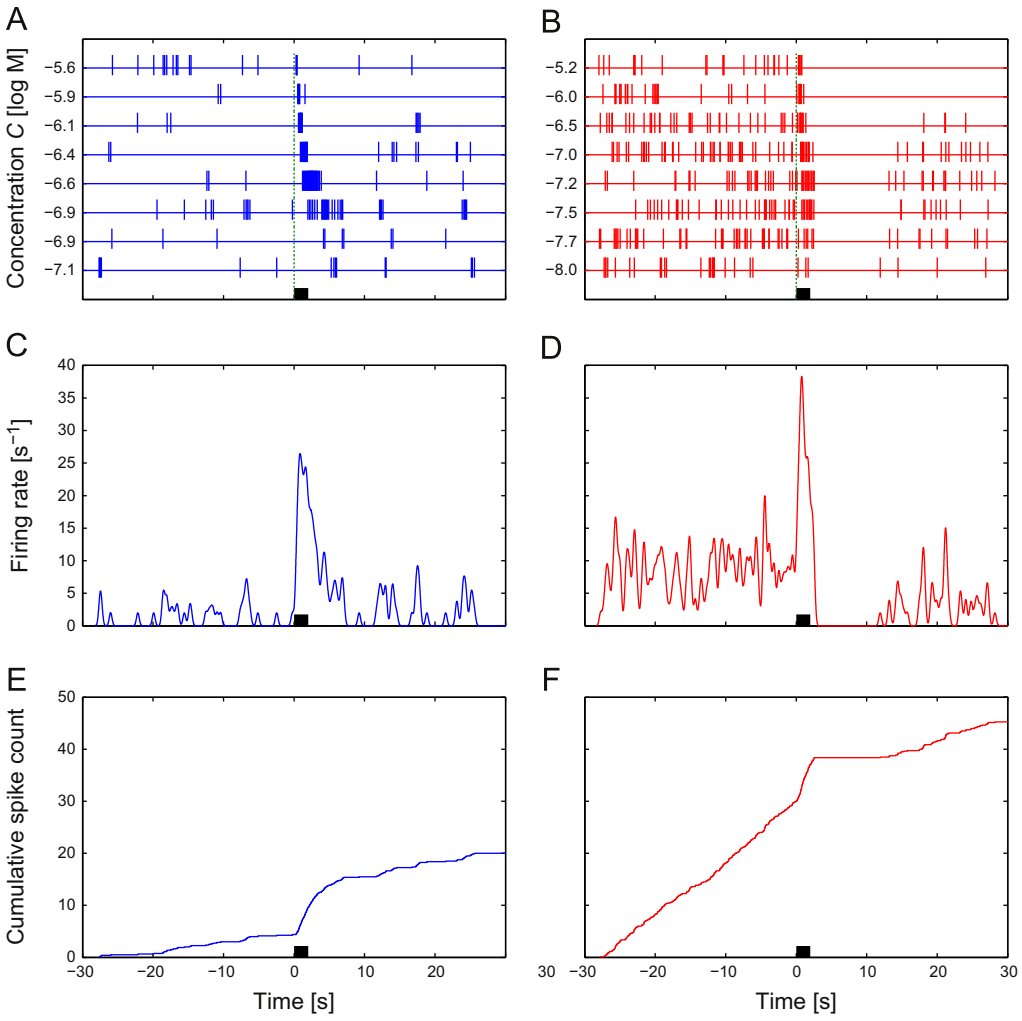

Fig. 1 – Examples of spontaneous and evoked activities in a set of records for a receptor neurons (RN #261, left column A, C, and E), a mitral cell (MC #743, right column B, D, and F), stimulated with ISO and LIM respectively. Top row (A and B): Each horizontal line shows the spike train recorded during 1 min. The thick bar on the time axis indicates the 2-s odor stimulation at concentration indicated on the left side (in log mole/L). Middle row (C and D) Kernel ($\sigma = 200$ ms) estimated firing rate of summated activity based on the set of records from the top row. It is equivalent to take the mean of the estimated firing rates of each trial or to estimate the firing rate of the spike train resulting from the summation of the individual trials and dividing by the number of the trials. Bottom row (E and F) Cumulative spike count normalized with respect to the number of records in the record set, indicating that the average numbers of spikes fired per record in the time window displayed were ca. 20 (RN) and 45 (MC).

Table 1 – Sample of odorants used.

Abb.[a]	CAS number[b]	Name	Formula	P (mmHg)[c]	M_{sat} (mole/L)[d]	C_{sat}[e]
CAM	76-22-2	Camphor	$C_{10}H_{16}O$	0.17	1.10×10^{-5}	−4.95
LIM	138-86-3	Limonene	$C_{10}H_{16}$	1.70	1.10×10^{-4}	−3.96
ANI	100-66-3	Anisole	C_7H_8O	3.06	1.98×10^{-4}	−3.70
ISO	123-92-2	Isoamyl acetate	$C_7H_{14}O_2$	3.77	2.44×10^{-4}	−3.61

[a] Abbreviated names used in this paper.
[b] Chemical abstract numbers.
[c] Saturating vapor pressures at $T = 295$ K.
[d] M_{sat}: molarity of saturating vapor, $M_{sat} = P/RT$ with $R = 62.364$ L mm Hg K^{-1} mol^{-1}.
[e] $C_{sat} = \log_{10} M_{sat}$.

Table 2 – Sizes of the samples studied.

Samples	Category[a]	Odorants[b]				Total
		ANI	CAM	ISO	LIM	
Animals	RN	6	6	7	2	21
	MC	7	15	7	2	31
Neurons	RN	19	9	9	3	40
	MC	11	25	12	6	54
Record sets[c]	RN	19	16	21	16	72
	MC	11	27	23	16	77
Records[d]	RN	158	95	146	151	550
	MC	118	274	232	160	784

[a] RNs (receptor neurons) and MCs (mitral cells).
[b] ANI (anisole), CAM (camphor), ISO (isoamyl acetate), LIM (limonene).
[c] A set of records with the same odorant applied to the same neuron at different concentrations.
[d] A ca. 1 min continuous recording before and after a single 2-s odorant stimulation.

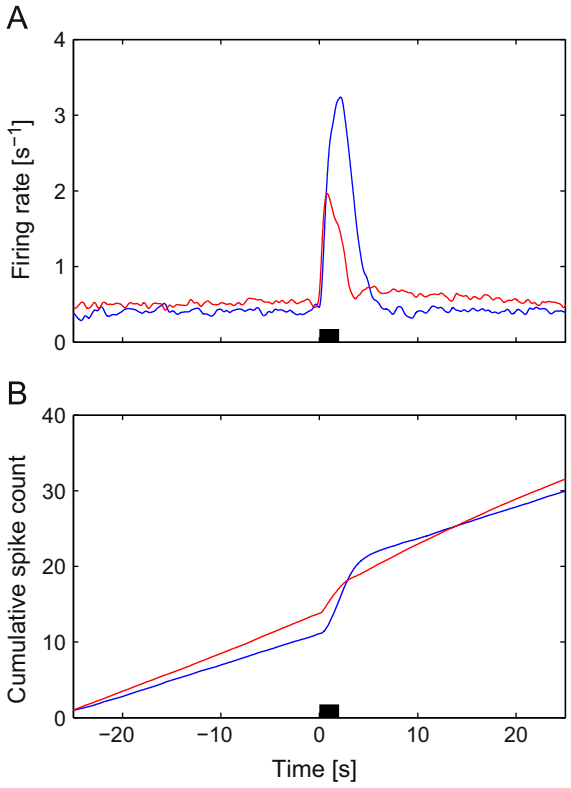

Fig. 2 – Temporal response curves of the two neuron categories, RNs (blue lines) and MCs (red lines), for all odorants and concentrations pooled together. (A) Kernel-estimated firing rate from −30 to 30 s with σ=200 ms. (B) Cumulative spike counts divided by the number of records showing both spontaneous and evoked activity. In both panels, the pre-stimulus curves are linear which indicates stationarity. The 2-s stimulation period (black box) triggers a peak in A and an abrupt change of the slope in B. The post-stimulus activity returns to its pre-stimulus value after less than 5 s for RNs but later for MCs, which is in agreement with the long lasting effect of ANI and LIM shown in Fig. 3B and D.

here because the small difference cumulates linearly over time with different slopes corresponding to different firing rates.

After stimulation, in both categories, the pooled activity increased with time, reached a maximum then declined in a more or less complex manner (Fig. 2A). The rate functions had a similar shape in both categories with a fast increase and a slower decrease. However, their values were again different. The post-stimulus peak of the firing rate was practically double, both in height and mid-height duration, in RNs than in MCs.

We repeated the same analysis for each odorant separately over all concentrations. In both RNs and MCs the maximum firing rate depended on the odorant and was highest for CAM and lowest for ISO. Also, in RNs and MCs stimulated with CAM and ISO the firing rate returned to its spontaneous level ca. 5 s after the onset of the stimulus but in MCs stimulated by ANI and LIM the return was complete only after ~20 s (Fig. 3).

2.2. *Concentration dependence of spike counts in single neurons*

Next, we examined how the activity of single neurons changed with odorant concentration. In RNs (Fig. 4A and B), the pattern of spikes fired after stimulation changes with the applied dose and we showed previously (Rospars et al., 2003) that several aspects of their responses – their latency, their duration, the number of spikes they include, and their firing frequency – depend on the dose. The MC responses (Fig. 4E and F) have apparently similar properties. To clarify these dose-dependent features and to compare them in RNs and MCs, we focus here on two of these aspects—the number of spikes and the firing frequency.

The height of the post-stimulus peak of the firing rate defined by the Gaussian kernel is a natural candidate for this analysis. We found that, for a given RN record set (that is a set of records from the same neuron to which the same odorant was applied at different concentrations), these peaks follow a sigmoid function of dose C (decimal logarithm of concentration) which, in most cases, can be described by a Hill function (not shown). However, the peak responses of single MCs are less easy to identify, especially at low concentration, because they can be confounded with spontaneous bursts. In order to avoid these uncertainties, we counted the number of spikes fired during 5 s after the onset of stimulation for each neuron–odorant-dose combination tested. This time window was decided based on the time course found above. A

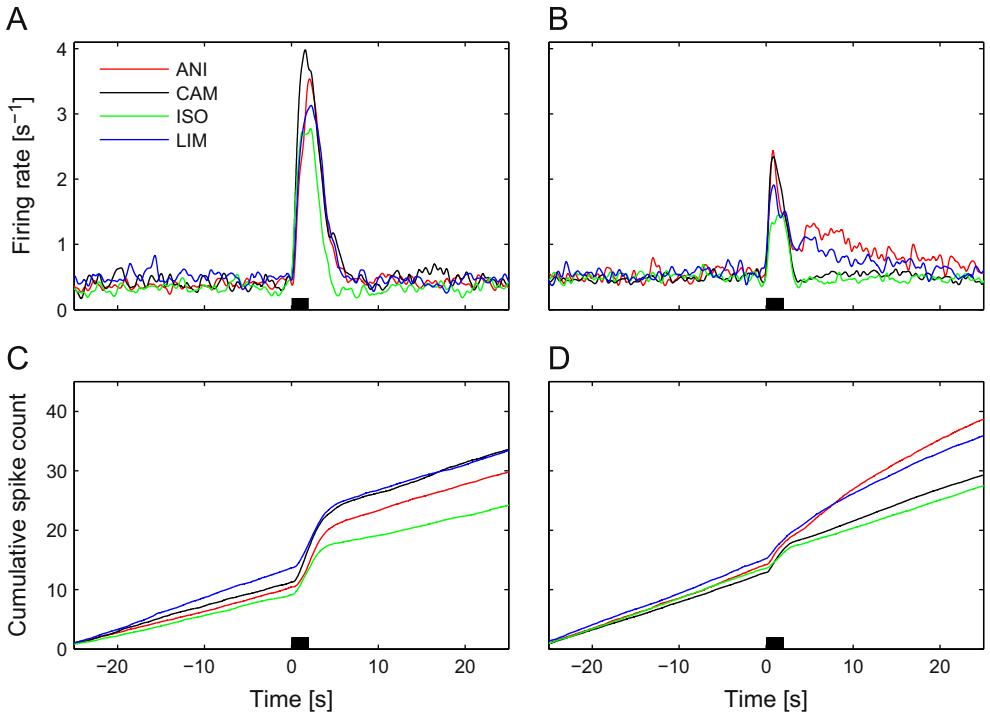

Fig. 3 – Temporal response curves analyzed per odorant with all concentrations pooled together. (A) Firing rate for RNs, (B) firing rate for MCs, and (C and D) cumulative spike counts for RNs (C) and MCs (D). In A and B, kernel is $\sigma = 200$ ms. Note the significant post-stimulus activity in MCs for ANI and LIM odorants in B and D. Thick line: 2-s stimulation period.

window shorter than 5 s would have not included all the spikes in the response and a window longer than 5 s would have included spikes belonging either to spontaneous activity or to an intermediate state in MCs stimulated by ANI and LIM. In both cases the counts would not reflect optimally the neuron response, whereas the 5-s time window includes all (or most of) action potentials fired between stimulus onset and full return to spontaneous activity.

The changes in the responses, in dependence on odorant doses, were investigated in 72 RN and 77 MC record sets. For each record set, the numbers of spikes N fired 5 s after stimulus onset were plotted as a function of dose C. Examples of dose–response plots are shown in Fig. 4C, D, G, and H. Typically, the plots are bell-shaped. N remains close to spontaneous activity at low doses (on average 2.5 ± 0.25 APs) until a threshold is reached, then rises quickly to a maximum within a short range of doses and finally returns slowly to spontaneous activity at high doses. However, for several record sets only the initial rising phase or, more rarely, the final falling phase were observed. In a few cases (2 for RNs and 8 for MCs) none of the phases could be discerned, the responses being seemingly independent of the dose or abnormally dispersed. These atypical record sets were removed from the samples.

To investigate the remaining plots we searched out a mathematical function linking N to C. The alpha function (Eq. (1) in Section 4) was found to give a reliable and easily interpretable description of the experimental points. Three parameters were determined for each record set—the threshold C_0, the maximum N_M and the dose C_M at which it is reached. These three parameters provide a complete description of the curves fitted to the experimental points. Examples of fittings are shown in Fig. 4. An intrinsic property of alpha functions is that the range of doses over which the curve increases (from C_0 to C_M) is ~5 times shorter than the range over which it decreases (say from C_M to dose C_S corresponding to 10% N_M, see Eq. (2)).

A remarkable property of $N(C)$ curves is their diversity as no two curves are identical. Together they tend to cover the whole range of odorant doses (from about –10 in RNs and –11 log M in MCs to C_{sat}) and the whole range of spike counts (from 0 to ~20 APs in RNs and to ~10 APs in MCs). This diversity can be precisely described by the distributions of the three parameters of the fitted alpha functions. In both RNs and MCs, we found that threshold C_0 follows a Gaussian distribution, and that C_M–C_0 and N_M follow lognormal distribution. This can be readily appreciated in Fig. 5 that shows the cumulative distributions of the parameters. It shows also that the distributions are significantly different in RNs and MCs. The threshold C_0 and the dose at maximum C_M are smaller by one log unit in MCs than in RNs, indicating that MCs are 10 times more sensitive than RNs. Also, the maximum count N_M is twice smaller in MCs than in RNs, indicating that the MCs are much less active in general than RNs.

2.3. *Concentration independence of firing rates and spike counts in neuron ensembles*

In the previous section responses in different record sets were studied separately. However, these analyses as summarized in Figs. 4 and 5 do not take into account the effect of different concentrations on global spiking activity of whole neuron ensembles. To see this effect, we followed a different approach where the responses in different classes of doses

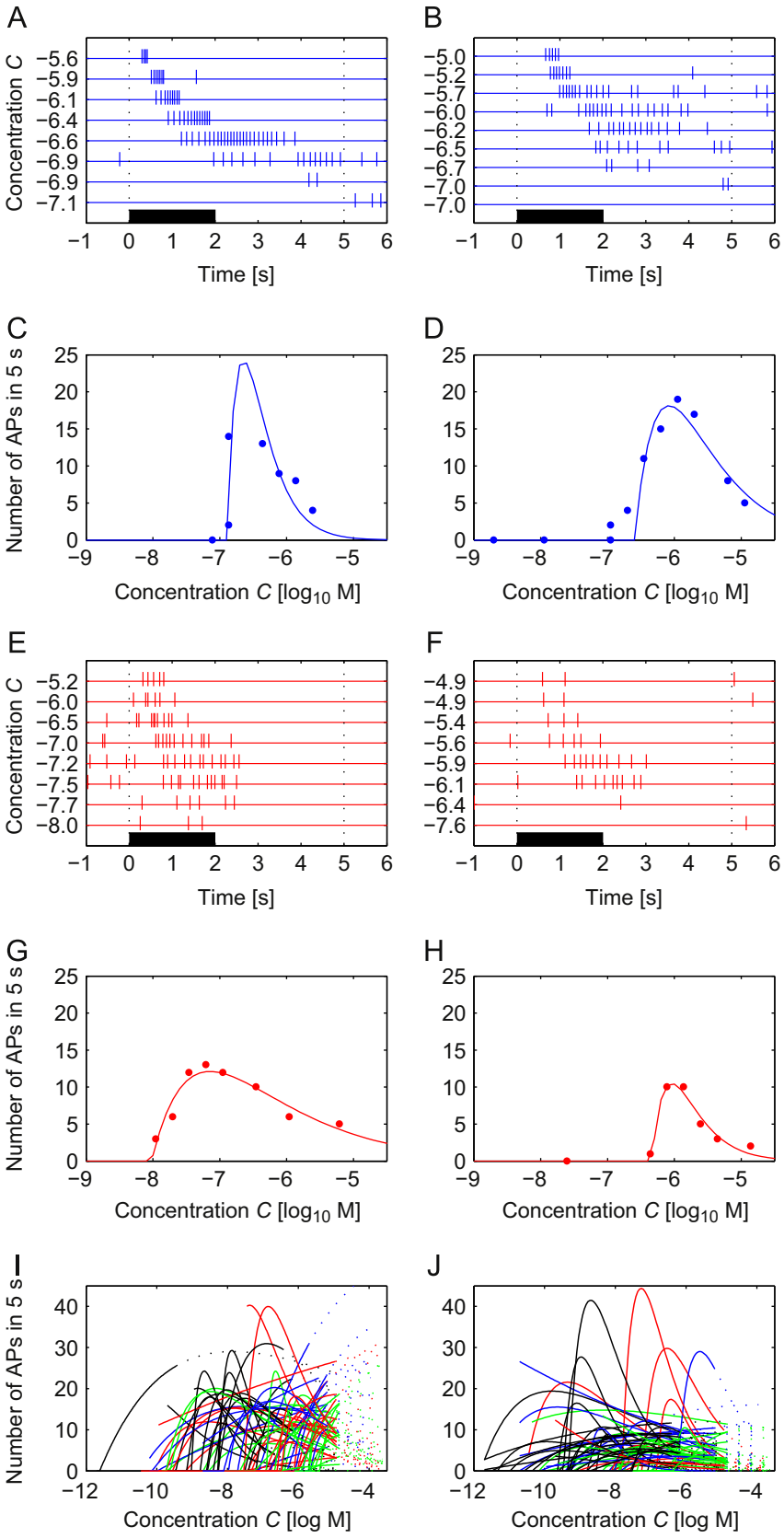

Fig. 4 – Dose–response plots for spike counts during 5 s $N(C)$ and fittings with alpha functions. (A) Record set RN #261 stimulated with ISO at 8 doses. Thick line: 2-s stimulation period. Vertical dashed lines: beginning and end of 5-s counting period. (B) Record set RN #521 stimulated with ANI at 10 doses (8 are shown). Same representation as in A. (C) Plot $N(C)$ corresponding to A with fitted alpha function. (D) Plot $N(C)$ corresponding to B. (E–H) Two examples of MCs, #743 stimulated with LIM at 8 doses (E and G) and #761 stimulated with ISO at 7 doses. Same representations as in A–D. (I) Page-filling property of RNs with all fitted alpha curves shown; dotted lines for part of curves beyond the last recorded response; curves colored as in Fig. 3 (red for ANI, etc.). (J) Page-filling property of MCs; same representation as in I.

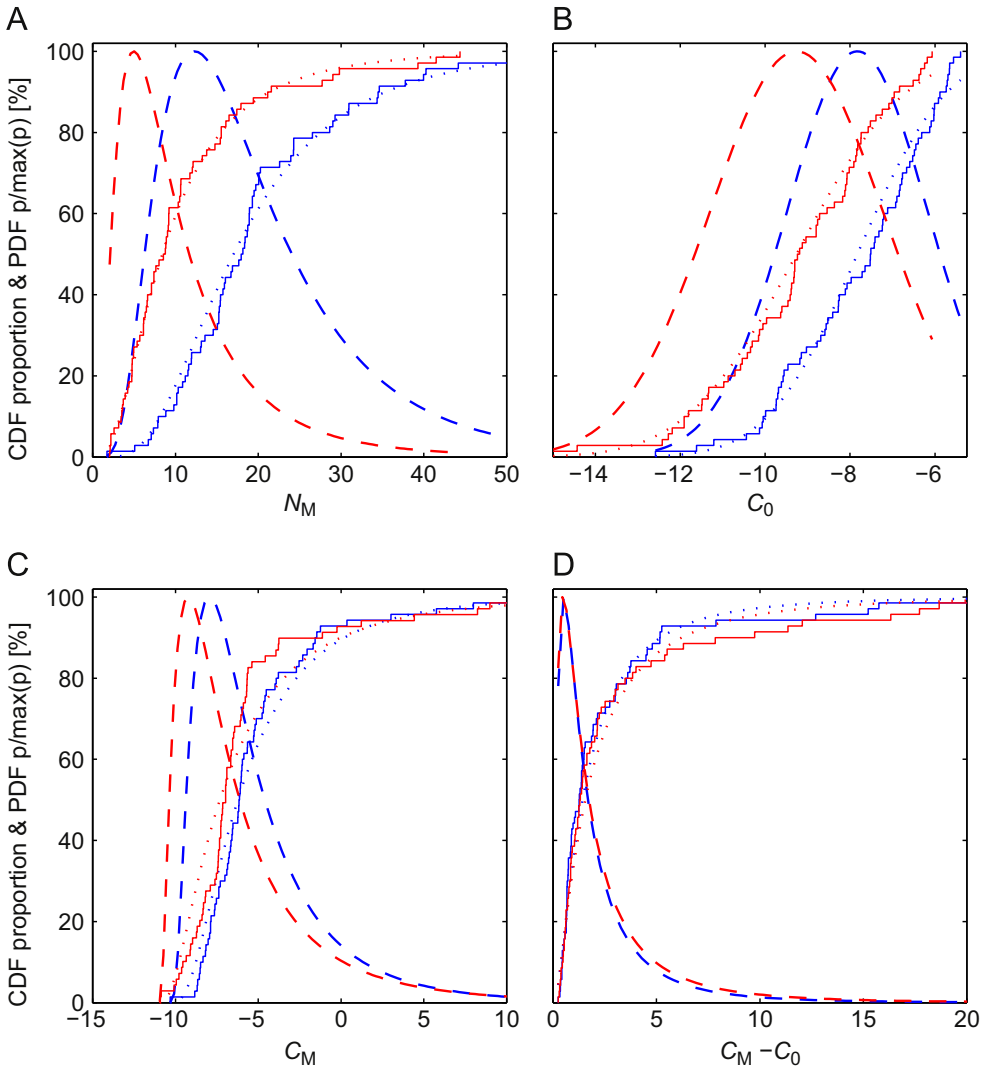

Fig. 5 – Distributions of the alpha function parameters: maximum N_M (A), dose at threshold C_0 (B), dose at maximum C_M (C) and dynamic range C_M–C_0 (D). In each plot RN distribution in blue (after removal of 2 neurons) and MC distribution in red (after removal of 8 neurons). For each parameter the empirical cumulative distribution function (CDF, staircase) and its fitted CDF and probability density function (PDF) are shown. The maximum of the PDF was adjusted to 100 to illustrate its shape (the actual values of the maxima are 0.17, 0.05, 0.24, 0.46, 0.11, 0.08, 0.20 and 0.42, respectively). The distributions of N_M, C_M and C_0 for RNs and MCs are significantly different; they are not significantly different for C_M–C_0 (Kolmogorov–Smirnov test at level 5%).

were studied separately employing, as in the previous section, firing rates and spike counts.

For establishing time-dependent properties we divided the available data in eight classes of doses with similar numbers of stimulations per class, from class 1 (lowest) to 8 (highest), with all odorants pooled together, and determined the firing rates (Fig. 6A and B). In RNs, the time courses were practically the same in all classes. However, in MCs, the time to response onset and the time to the peak of the firing rate decreased with increasing concentration. Remarkably, the heights of the peak following the stimulations were not related to the concentration (Fig. 6C and D) contrary to what is observed in single RNs (e.g. Rospars et al., 2003).

Next, to confirm this unexpected behavior we used spike counts within a 5-s time window. We divided the whole range of doses in seven equal classes (bin width 1 log M each). In each class, the individual counts were summarized as their median and interquartile range (IQR, which contains 50% of the data). Plots of these numbers as a function of odorant dose, after pooling the odorants together (Fig. 7A), show that the total activity does not change systematically with dose, as the slopes of the regression lines of counts on concentration for RNs and MCs are not significantly different from zero. This indicates that the total number of action potentials fired per recorded neuron in response to an odorant is practically independent of its concentration. Similar plots for different time windows (2 and 15 s not shown, 30 s shown in Fig. 7B) and per odorant (not shown) revealed the same robust independence on concentration (for MCs at 30 s the slope is even negative and significantly different from zero).

We reasoned that the observed dose invariance was the consequence of two features of the $N(C)$ curves as described by alpha function (see Eq. (1)): the diversity of their thresholds and the decreasing number of spikes fired at high doses. To

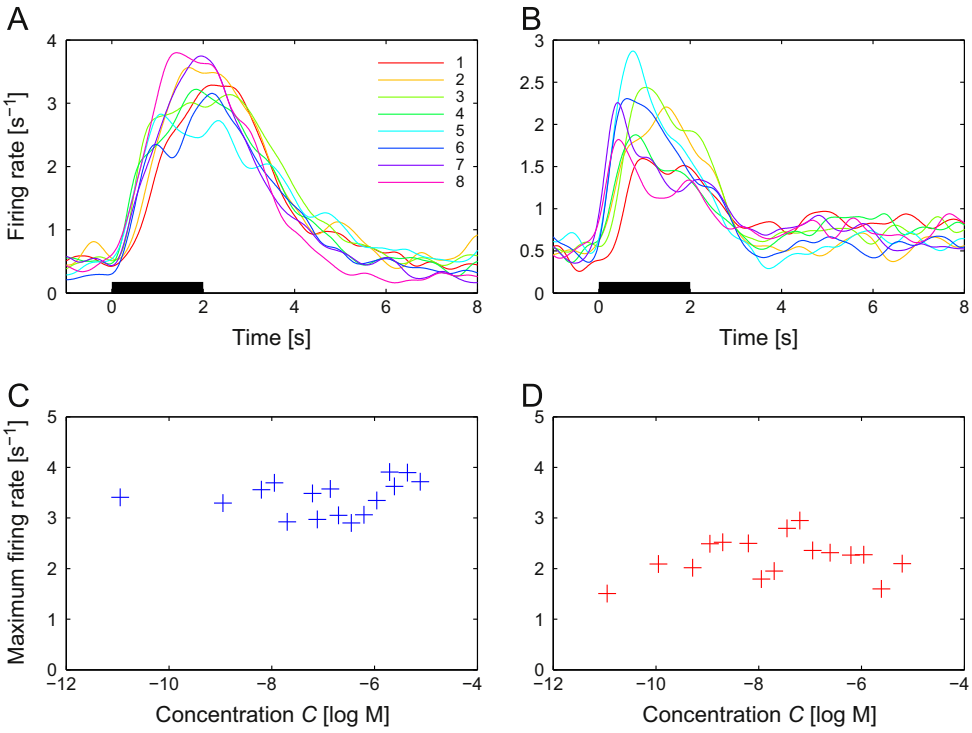

Fig. 6 – Temporal response curves of neuron ensembles (A and B) and maximum response (C and D) based on kernel-estimated firing rate (σ=200 ms) for different classes of odorant concentrations. (A) Average firing rates of RNs during and after odorant stimulation in 8 classes of concentration from 1 (lowest) to 8 (highest), with all odorants pooled together. The classes were defined in order to include approximately the same number of records. Boundaries of classes (in log M): 1 [−10.95 to −8.20], 2 [−8.20 to −7.70], 3 [−7.70 to −7.11], 4 [−7.11 to −6.70], 5 [−6.70 to −6.21], 6 [−6.21 to −5.71], 7 [−5.71 to −5.36], and 8 [−5.36 to −4.86] with 67, 61, 72, 74, 58, 79, 65, 63 records per class respectively. (B) Same representation as A for MC category, class boundaries [−10.95, −9.29, −8.70, −7.95, −7.45, −6.95, −6.21, −5.61, and −4.86] with 98, 91, 104, 99, 85, 107, 99, and 81 records respectively. (C) Maximum firing rate of 16 RN curves (similar as those shown in A) as a function of the left boundary of each of the 16 concentration classes. The regression line (not shown) is F_{max}=3.736+0.052C. The slope is not significantly different from zero (t-test, p=0.39). (D) Same representation as C for MC curves. Regression line (not shown): F_{max}=2.524+0.040C; slope not significantly different from zero (t-test, p=0.55).

check this hypothesis, first, we replaced the experimental points with their fitted alpha functions (70 for RNs and 69 for MCs). We determined the numbers of spikes fired by the two categories and summarized them as the median and IQR in each of the seven classes. Again, the results were almost independent of the dose (Fig. 7C and D). Second, we went one step further and developed a model of the neuron populations. For these simulations, the parameters (C_0, C_M–C_0 and N_M) of alpha functions were drawn independently at random according to the statistical distributions defined previously in Fig. 5. Owing to the large number of random drawings (5000) it was possible to analyze the results with narrower dose classes (length 0.25 log M each) than in the actual experiments. The results obtained are consistent with a constant or slowly decreasing activity per recorded neuron (Fig. 7E and F).

3. Discussion

3.1. *Frequency coding*

When stimulated many characteristics of the spike train fired by a neuron, whether of first- (RN) or second-order (MC) are modified. Typically RNs and MCs respond to odorant stimulation with a sudden increase of their firing rate followed by a decrease. It is thus possible, at least in principle, to define the starting and ending time of the response and consequently its duration, the number of spikes it includes, the firing frequency (for example the maximum instantaneous frequency) and the response latency (from stimulus onset to response onset) (Rospars et al., 2003). However, this method can present difficulties when the odorant dose applied and the corresponding response are weak. This is especially the case in frog MCs for which the spontaneous activity is higher than in RNs (Rospars et al., 1994) and the responses twice lower (the present work), so compounding the sources of noise. Because it proved difficult to define reliably "responding spikes" in MCs we turned to the less demanding spike count method. A significant advantage of using spike counts in a fixed time window is to minimize the effect of erroneous determination of the starting and ending time of the response in each trial and to increase the number of usable recordings. Although, the price to pay for this robustness is obvious (a single count versus at least four characteristics) it seems appropriate for establishing the general properties of the two neuron populations.

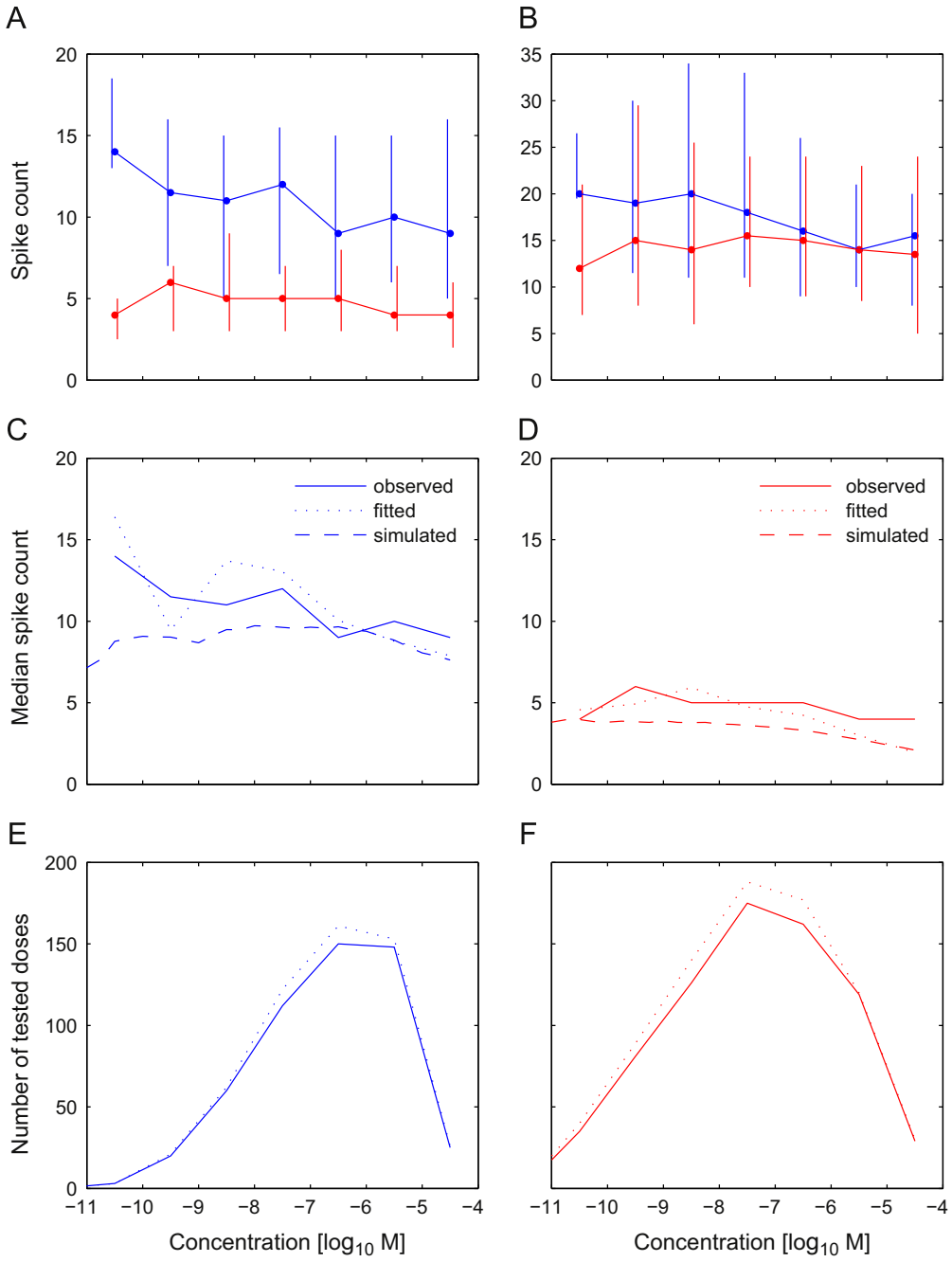

Fig. 7 – Dose–invariant plots of the two neuron categories RNs (blue lines) and MCs (red) for all odorants pooled together. (A) Concentration axis divided in seven classes of 1 log M width. Responses quantified as spike counts N per record during 5 s after stimulus onset. The spike counts in each class (records with $N=0$ were not included) are represented by their median and interquartile range (vertical bar); both are practically independent from concentration. The regression lines (not shown) are $N=11.99-0.22C$ for RNs and $N=6.59-0.083C$ for MCs. The slopes are not significantly different from zero (t-test, $p=0.38$ for RNs and $p=0.55$ for MCs). (B) Same representation as A for spike counts during 30 s after stimulus onset. For RNs the regression line is $N=28.38-1.75C$; the slope is significantly different from zero ($p<10^{-4}$) indicating that counts even decrease with concentrations. For MCs, $N=19.86-0.091C$; the slope is not significantly different from zero ($p=0.820$). (C) Comparison for RNs of the median spike counts during 5 s for experimental values N (same as in A), for the 70 alpha functions fitted to the experimental points (see Fig. 4) and for a model simulating 5000 alpha functions based on the distributions of the parameters N_M, C_0 and C_M–C_0 (see Fig. 5) with classes of 0.25 log M width. (D) Same representation as C for MCs. (E) Number n of experimentally tested doses (or spike counts) for RNs either with $N=0$ included (dotted) or not (solid). (F) Same representation as E for MCs.

So, in practice, even such a simple concept as the firing rate of a response is not easy to define and manipulate. This is the reason why we used two complementary characteristics: spike count in preselected time windows and Gaussian kernel estimates of the instantaneous firing frequency. Instantaneous frequency, because it shows how the firing rate changes with time, is richer but more difficult to evaluate and more sensitive to the amount of experimental data available; it appeared invaluable for the analysis of neuron ensembles (Section 2). Spike counts, although they depend on the selection of the time window and are insensitive to sudden fluctuations of the firing rate, proved the most suitable to analyze single neuron responses (Section 3).

3.2. *Time dependency of firing frequency*

For all tested concentrations pooled together, the rate functions of the two neuron categories present two clear distinguishing features. First, the peak of firing rate in MCs is ~60% of that in RNs and returns more quickly to spontaneous activity (see Fig. 2) which is higher in MCs (~20%) than in RNs. The peak response is also reached ~50% earlier in MCs than in RNs (Fig. 2). Second, the falling phase, which follows the initial peak, and the rising phase is nearly symmetrical to the rising phase in RNs for all odorants, but asymmetrical in MCs neurons for some odorants because of a long lasting excitation (Fig. 3). So, in both cases, the falling phase continues well after the stimulus offset (Duchamp-Viret et al., 1990; Mazor and Laurent, 2005; Namiki and Kanzaki, 2011).

The first property indicates that MCs are less active than RNs at the same concentration: they utilize less action potentials and consequently less energy for coding the same stimuli (see below). The second property implies that the falling phase of a MC is shaped by their intrinsic properties or the synaptic activity of the surrounding neurons in the olfactory bulb network, particularly the inhibitory synapses.

It is also worth noting that the maximum firing rate of first- and second-order olfactory neurons is much smaller in vertebrates (13–50 AP/s in RNs, Rospars et al., 2003, 2008; ~20 AP/s in MCs, Duchamp-Viret and Duchamp, 1997; this work) than in insects (100–300 AP/s in RNs, 50–250 AP/s in PNs, e.g. Bhandawat et al., 2007; Ito et al., 2009). These large differences remain to be interpreted.

3.3. *Dose dependency of spike counts in single neurons*

The number of spikes fired in a fixed 5-s post-stimulus time window was found in most neurons to depend non-monotonically on the dose with a well defined threshold, a fast rise and a slower decline. This curve was found to be reasonably well described by an alpha function, which is one of the simplest functions with this overall behavior. We are not aware of any physiological model predicting this behavior, so this description is purely empirical at the present time. However it is in good agreement with our previous finding that the number of spikes in the "response window" is an alpha function of the dose in RNs (Rospars et al., 2003). This good agreement could be expected on the conditions that (i) the 5-s fixed window includes the peak response, and (ii) the number of spikes fired after the response returns to the spontaneous activity observed before the response and is practically negligible with respect to the evoked activity.

The present results confirm what we found previously for the evoked number of spikes in RNs, that is the alpha dose-dependency, the page-filling property, the lognormal distribution of the maxima N_M of the alpha functions and of the range C_M–C_0. Two of these properties – the diversity of firing thresholds and the decrease in the number of spikes at higher concentrations – have been observed also in an insect (Ito et al., 2009). However, with more data points available, the distribution of C_0 was here corrected; it is not uniform but more likely Gaussian. The distributions shown in Fig. 5 must not be overinterpreted. The values of the parameters for the incompletely observed curves – those with only rising of falling phases visible – permit to give a proposed description of the $N(C)$ curves in the experimentally studied range of doses but, contrary to the complete curves, it cannot be ascertained that their estimated threshold C_0 is really the threshold of the neuron for the odorant tested.

The results on RNs were here extended to MCs. We showed that the $N(C)$ curves of MCs are also alpha functions of dose C and that the distributions of their parameters are qualitatively the same for MCs as for RNs. However, the characteristics of the distributions are different for RNs and MCs. The MC curves are shifted to the left on the dose axis by ~1.4 log M with respect to RN curves, as shown by C_0 and C_M, which means that they are ~25 times more sensitive. The increase in sensitivity can be readily interpreted as resulting from the convergence of many RNs on each MC (Van Drongelen et al., 1978; Duchamp-Viret et al., 1989; Byrd and Burd, 1991; Rospars and Fort, 1994). The maximum number of spikes fired are twice smaller in MCs than in RNs ($\exp(2.8340)/\exp(2.1287)=2$, see Figs. 2 and 5). The dynamic ranges $C_M - C_0$ are only ~10% wider in MCs than in RNs. The same striking page-filling property observed in RNs (Rospars et al., 2003) was now extended to MCs. So, the only conspicuous change of the MC responses with respect to the RN responses is an increase in sensitivity without obvious changes of the almost uniform and dense coverage of the C–N space.

As intensity encoder the number of spikes fired presents two drawbacks: it increases from threshold to peak on a short dynamic range C_M–C_0 and it is ambiguous as it takes the same value at two different concentrations. This later property stands in contrast with latency and peak instantaneous frequency that both evolves monotonically with increasing doses (Rospars et al., 2003). So, individual neurons can obtain an unambiguous measure of the dose based on L and F while N can extend their dynamic range if the overall range ΔC is taken into account. Although it is doubtful these properties are directly used to code odorant concentration it can be argued that they play an indirect role as discussed in the next subsection.

As seen above, MCs are intrinsically less active than ORNs at the same concentration: they need less action potentials and consequently less energy for coding the same stimuli. This single-neuron effect is compounded with the convergence of many RNs per MC (from 34:1 to 200:1 depending on MCs, Jiang and Holley, 1992; Duchamp-Viret and Duchamp, 1997), and is likely not compensated by the fact that MCs are less finely tuned to odors than RNs. Overall, for the same

stimulation, it may be expected that the total number of spikes fired in the MC population is lower than that in the RN population. This is in accordance with Barlow's (Barlow, 1969) "economy of impulses" which expresses the tendency for successive neural layers to use lower and lower levels of cell firings to produce equivalent encodings.

3.4. *Dose-invariant coding in neuron ensembles*

We have found a near constancy of the maximum firing rate (Fig. 6) and of the median number of spikes fired in a given time window (Fig. 7) at different concentrations. The same property was observed previously in a sample of PNs (analog to MCs) in a locust when stimulated by different odorants at different concentrations (Stopfer et al., 2003).

In the frog, this property results from the different thresholds of the neurons and the specific pattern of spikes at different doses described above (with rise and fall). It is intuitive that these two properties can compensate one another and maintain more or less constant the total number of spikes fired all along the dose axis. We verified this expectation with models taking into account the Gaussian distribution of the thresholds and the alpha dependence of N on dose in each neuron.

This means that the energy E consumed *per* "*typical*" (*median*) *recorded* neuron is nearly constant, independent of the odorant concentration. Is it possible to go further and to interpret these results in terms of population coding and global energy consumption? Besides efficient information processing, energy consumption is a strong constraint because neural tissues are metabolically expensive, which might favor spike-saving codes (Aiello and Wheeler, 1995; Sokoloff, 1989 and references given in Section 1).

First of all it must be realized that the neurons (RNs or MCs) that never responded to any of the odorants at any concentration were not taken into account. Therefore, the reference ensemble P is the subset of neurons (RN or MC) that could respond to the tested odorants (the responding neurons). It is known by other experiments that neurons exist that do not respond to any of these odorants. What proportion of the complete population the responding ensemble P represents is outside the scope of this paper.

Now, two extreme assumptions can be made with respect to ensemble P:

(1) The first assumption is to consider that the neurons of P were recorded at random, that is with uniform sampling of the tested doses C, with no preference for mid-range doses for example. Then the samples studied would be representative of the ensemble and the constancy of the spike counts would be an intrinsic property of P. Under this assumption the number of neurons of P able to respond is the same at any dose, let's say K. As a result, the energy consumed by the ensemble is constant ($K \times E$) at any dose.

(2) The opposite assumption is to consider that the concentrations tested were not randomly selected but reflected the number n of neurons that were able to respond at a given dose. Then the number n of neurons tested would vary with C. In this extreme case, the energy consumed by the ensemble is ($n \times E$) and therefore varies with the dose like n.

Assumption (1) can be rejected for two reasons. First, there was no attempt to sample uniformly the dose axis. On the contrary the experimental protocol aimed at deciding whether a recorded neuron (usually with spontaneous activity) was responding strongly enough to at least one of the odorants at relatively high dose to justify further investigations; in this case (and only in this case) the threshold was estimated and then a series of increasing doses was applied. The doses tested were thus decided by the sensitivity of the neuron in order to maximize the number of usable responses. Second, it can be shown a posteriori that the number n of stimulations (and corresponding recordings) increases almost linearly with the dose then declines at high doses (see Fig. 7E and D). If the sampling was uniform, n would be constant ($n=K$). In conclusion, assumption (2) is likely closer to reality.

According to this assumption and knowing that E is constant, the total energy consumed by ensemble P should be proportional to n and so increase from C_{min} (ca. 10^{-10} M for RNs, and 10^{-11} M for MCs) to C_{max} (ca. 10^{-6} M in RNs and 10^{-5} M in MCs). The subsequent decline from C_{max} to C_{sat} may be a sampling effect because stimulations at very high doses were avoided as strongly stimulated neurons take a long time to return to their resting state. The initial increase is in agreement with experimental observations with calcium imaging showing that when concentration increases not only the activity of RNs converging onto a glomerulus increases but also additional glomeruli are activated (Oka et al., 2006; Nawroth et al., 2007; Carey et al., 2009; Münch et al., 2013; see also Fletcher et al. 2009).

In summary, the properties studied here of RNs and MCs are remarkably similar. The main transformation occurring in the olfactory–bulb synaptic network is an increase in sensitivity of MCs with respect to RNs and a probable decrease in the total number of action potentials required to encode the olfactory message. Surprisingly, the total number of action potentials fired by recorded neurons, and hence their energy consumption, is constant (independent of concentration). However the number of active neuron is likely concentration-dependent so that the total energy consumption may be expected to be also concentration-dependent.

4. Experimental procedures

4.1. *Animal preparation*

The experiments were carried out on frogs (*Rana ridibunda*) in accordance with the European Communities Council Directive for the care and use of laboratory animals. Animals were locally anesthetized with xylocaine (lidocaine 2%) and immobilized by a subcutaneous injection of 0.1 ml of d-tubocurarine (0.2%). They were wrapped in wet gauze to preserve skin respiration and kept at constant temperature (13 °C) throughout the experiments (Duchamp et al., 1974). The mucosa was dissected on a single side. A lateral

rectangular incision was made from the nostril to the base of the orbit in an area devoid of sensory epithelium; thus, the totality of the olfactory epithelium was preserved. The ipsilateral olfactory bulb was uncovered by perforating the cranial wall and the meninges were dissected. A constant flow of moistened pure air was continuously flowed on the preparation.

4.2. *Stimulation and electrophysiological recordings*

Activities of neurons of the epithelium and bulb were recorded with extracellular glass microelectrodes filled with an alloy of Wood's metal (80%) and indium (20%) (Gesteland et al., 1959). Their impedance was adjusted between 1 and 4 M at 1 kHz by electrolytical plating of the tip in a solution of platinum tetrachloride (diameter at the tip ~2 μm). The common electrode was an Ag/AgCl plate placed into the frog's mouth. Signals were amplified (bandwidth, 0.3–3 kHz; input impedance, 500 MΩ).

The ORNs were recorded in all regions of the ventral olfactory epithelium, at a depth of 50–270 μm from the external surface of the mucous layer. MCs were recorded in the anterior part of the bulb where the somata of MCs are located in a frontal plane (Northcutt and Royce, 1975; Scalia, 1976). The microelectrode was inserted vertically in this region at a depth of 300–1,200 μm. The bulbar units recorded were identified as output neurons by means of a collision test showing that their axons project into the lateral olfactory tract and therefore are second-order neurons (Duchamp-Viret et al., 1989).

Interspike intervals (ISIs) were measured off-line with a resolution of 1 ms. All recordings that might have involved more than one neuron were discarded. An excellent reproducibility of responses was found in repeated stimulations with the same odor at the same concentration for 1 h or more. Note however that this time was not long enough to routinely repeat all stimulations.

For every stimulation the neuron was recorded 30 s before and after the stimulation onset (Fig. 1A and B). The interval between two successive stimulations was 2 to 4 min depending on the stimulus concentration. Four odorants were tested, anisole, DL-camphor, isoamyl acetate and DL-limonene (highest purity available, Merck, France). These compounds were chosen for their efficacy to stimulate ORNs and as representative of previously identified odorant groups (Duchamp et al., 1974; Revial et al., 1983; Duchamp and Sicard, 1984; Sicard and Holley, 1984). The odorants were delivered as almost square pulses of 2 s duration with precisely controlled concentrations and time course (rising and falling time constants, 0.22 and 0.26 s respectively). The olfactometer (Vigouroux et al., 1988) could deliver 20 different concentrations, characterized by their *relative concentration index I*, each concentration being 1.778 larger than the previous one (4 concentrations per decade, $10^{0.25}=1.778$) in the range 10^{-6} of saturating vapor ($I=1$) to 5.62×10^{-2} ($I=20$). The index of all saturated vapors is $I=25$.

Throughout this paper, we use the *dose* scale $C=\log_{10}M$ with M in mole/L. The molarity M_{sat} and corresponding dose C_{sat} of the saturated vapors at 22 °C are given in Table 1. The dose C of a vapor of index I is $C=C_{sat}+(I-25)/4$. The difference

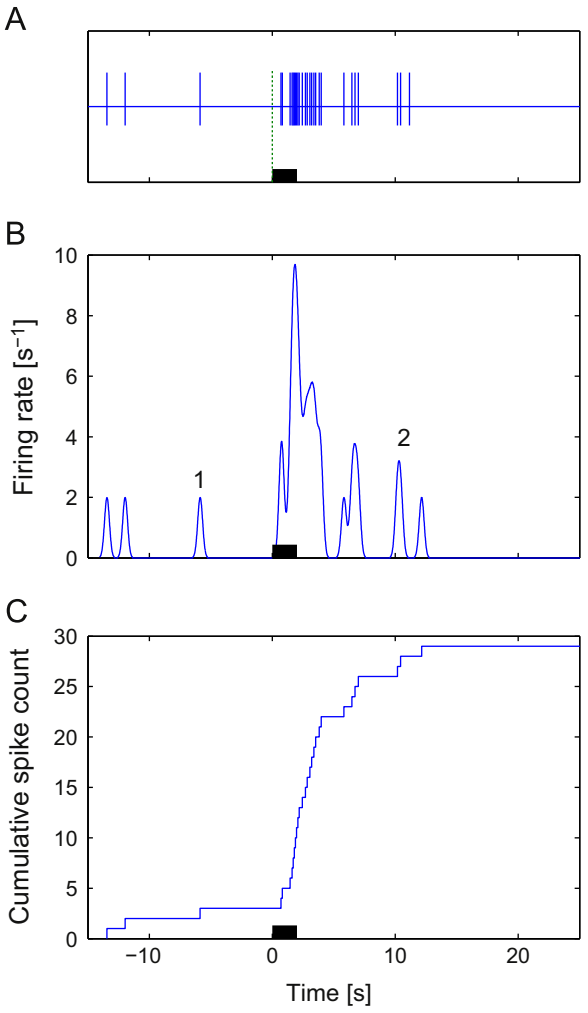

Fig. 8 – Estimation of response frequency. (A) Example of recorded spike train from RN #521 stimulated with odorant ANI at concentration $10^{-5.95}$ mol/L. (B) Kernel-estimated firing rate $\lambda(t)$ of the spike train shown in A. Each spike in the recorded spike train (A) is replaced by a kernel function, here a Gaussian function of standard deviation $\sigma=200$ ms. The rate function is obtained by taking the sum of all Gaussians. For example the area under the two overlapping Gaussians (labeled "2" on the right) is twice the area under the isolated Gaussian (labeled "1"). (C) Cumulative spike count starting 15 s before stimulus onset. Response is seen as an abrupt change in the slope of the curve. In all panels the thick bar on the time axis displays the time and duration of the odorant stimulation.

in the scales is mainly noticeable for camphor because it is the least volatile compound, with a vapor ten times less concentrated than the three other compounds.

The mean value of the strongest applied stimulations was −6.8 log M for camphor and was close to −5.2 log M for limonene, isoamyl acetate and anisole, which shows that camphor was farther from the physical limit C_{sat} imposed by vapor saturation (−4.95 log M) than the other odors (−3.8 log M), for which almost the whole range of stimuli from the weakest (limited by neuron sensitivity) to the strongest (limited by the volatility of odorants) was explored.

4.3. *Estimation of firing rate functions using Gaussian kernel*

To determine the probability that a neuron fires an action potential (or rate function) we used the kernel method which is an extension of the PSTH method. Beyond technical advantages, the main feature of this method is that it integrates all aspects of the neuron responses, not only the initial excitatory response but also the following silent period and the eventual final rebound after the silent period. This is a major difference with our previous studies, which took into account only the initial excitatory part (Rospars et al., 2003, 2008) or even only the firing rate (Sandström et al., 2009).

The spike rate is a function of time $\lambda(t)$ such that the mean number of spikes in a time interval is equal to the integral of this function. For small Δt, $\lambda(t)\Delta t$ is the probability of observing a spike in a short interval close to t. The time varying rate function was estimated by using the kernel method which is based on convolution of the spike train with an appropriate kernel function (Sanderson, 1980; Richmond et al., 1990; Szücs, 1998; Nawrot et al., 1999; reviewed in Kass et al., 2005). Consider a spike train (prestimulus activity as well as evoked activity) with spikes occurring at times $t_1,\ldots,t_n$. The estimate of the rate function $\lambda(t)$ is defined as $\lambda(t)=\sum_{i=1}^{N}K(t-t_i)$. The Gaussian function of standard deviation σ was used as kernel $K(t)$. The method is illustrated in Figs. 1C and D and 8B. The only free parameter in the method is the width σ of the kernel. Fig. 9 shows how $\lambda(t)$ depends on σ in our data. The estimated $\lambda(t)$ was calculated for the summation of all 550 recordings of ORNs, including all odorants and doses tested. The only effect of increasing σ is to reduce the fluctuations in $\lambda(t)$. The firing rate of spontaneous activity is the same whatever σ, about 0.5 spike/s. The peaks corresponding to stimulated activities remain also the same in height (~3.5 spikes/s) and duration (~5 s). For all studies in the present paper, we chose $\sigma=200$ ms. With this value, knowing that 95% of the area below a Gaussian curve is included within $\pm 2\sigma$ from the mean, a neuron firing at a constant rate of 1.25 spikes/s or less (ISI > 0.8 s or $>4\sigma$) would yields $\lambda(t)$ formed of almost discrete Gaussian curves; and at a constant rate of 5 spikes/s or more, it would yield more or less constant $\lambda(t)$. The rate 5 spikes/s is half the average maximum firing rate observed for ORNs in Rospars et al. (2003).

4.4. *Cumulative spike count*

The firing rate function expresses neural activity at a given time (often called instantaneous firing rate). To compare neural activity in different time periods it is also convenient to consider the integral $\Lambda(t)$ of the rate function $\lambda(t)$ which is equivalent to the total number of spikes fired in a selected period. $\Lambda(t)$ is illustrated for a single spike train (Fig. 8C) and for single record sets (Fig. 1E and F). For easier comparison in different samples the cumulative spike counts were normalized by dividing by the size of each sample. The firing rate $\lambda(t)$ (parallel to probability density function) and the cumulative spike count $\Lambda(t)$ (parallel to cumulative distribution function) give two equivalent and complementary views.

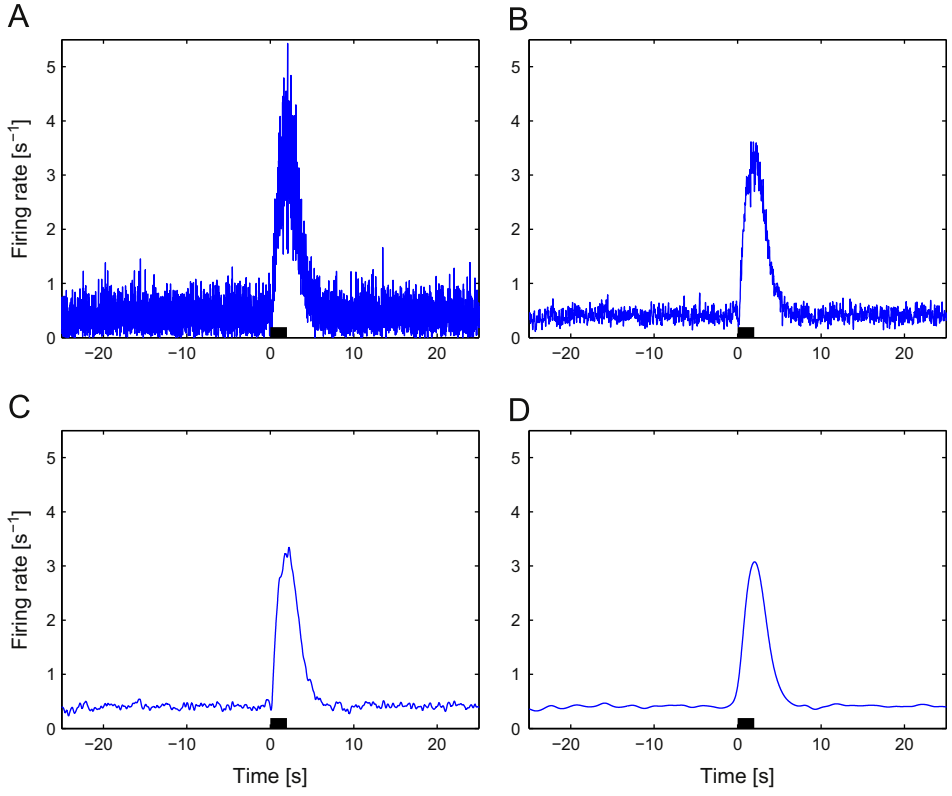

Fig. 9 – Effect of the width σ of the kernel on the estimation of firing rate based on all 550 records of RNs irrespective of odorant and concentration. Kernel widths: 4 ms (A), 20 ms (B), 100 ms (C) and 500 ms (D). For $\sigma \geq 20$ ms the rates estimated are practically the same but the curve becomes smoother.

4.5. *Fitting of spike counts to odorant dose*

The best fittings of the number $N=\Lambda(t_1)-\Lambda(t_0)$ of spikes fired in a given time window (t_0, t_1) were obtained with the alpha function which can be written as

$$N(C) = N_M \frac{C-C_0}{C_M-C_0} \exp\left(1-\frac{C-C_0}{C_M-C_0}\right), \quad C \geq C_0 \qquad (1)$$

with three parameters: the threshold C_0, the maximum N_M at the dose C_M (Fig. 10). All three parameters were estimated from data using a nonlinear regression program (nlinfit, Matlab, The Mathworks, Natick, USA).

The dynamic range of ΔC of N can be defined as the distance between C_0 at which $N(C)$ starts to rise and the dose at which it crosses downwards a predefined level, e.g. 10% of its maximum N_M, or a predefined dose, e.g. C_{sat}. It can be shown that at the 10% level the dynamic range is

$$\Delta C = 4.89(C_M-C_0) \qquad (2)$$

This is an intrinsic property of the alpha function that ΔC is ~5 times longer than the rising phase C_M-C_0, or that the rising and falling phase are ca. 20% and 80% of ΔC respectively.

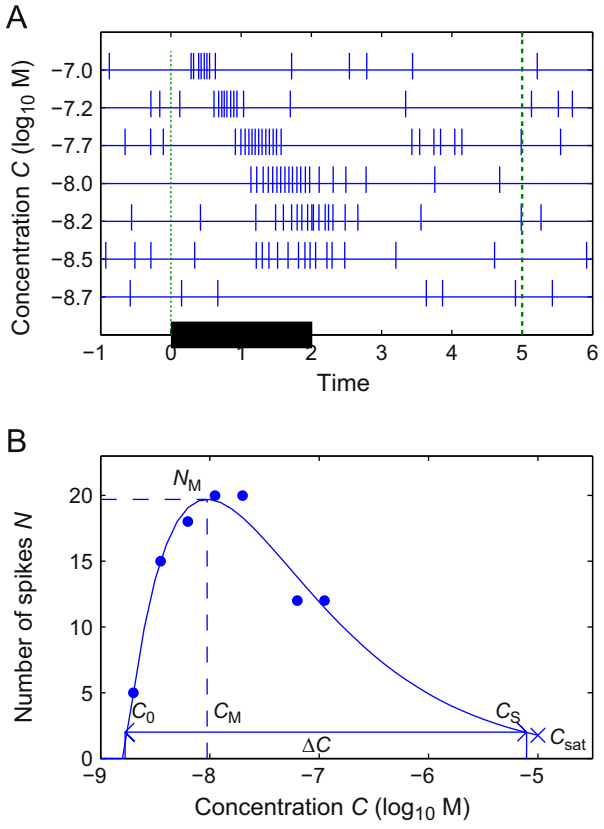

Fig. 10 – Alpha function (defined by Eq. (1)) describing the number of spikes N fired during a fixed time window (5 s in this example) as a function of dose $C=\log_{10}$ concentration (M). (A) Record set RN #361 stimulated with CAM at 7 doses, same representation as Fig. 4. (B) Alpha function fitted to spike counts found in A. Threshold C_0, dose C_M at maximum N_M, dose C_S at 10% of N_M, dynamic range $\Delta C=C_S-C_0$ (obeys Eq. (2)) and dose C_{sat} of the saturating vapor (cross).

Acknowledgments

We thank three anonymous referees for helpful comments. JPR was funded by INRA and the State Program "Investissements d'avenir" managed by Agence Nationale de la Recherche (Grant ANR-10-BINF-05 "Pherotaxis"). PL and PS were supported by Center for Neurosciences P304/12/G069, Grant no. RVO:67985823, and the Grant Agency of the Czech Republic, Project no. P103/11/0282. PDV was funded by CNRS and Université Claude Bernard, Lyon.

REFERENCES

Abbott, L.F., Luo, SX, 2007. A step toward optimal coding in olfaction. Nat. Neurosci. 10, 1342–1343.
Adrian, E.D., 1950. Sensory discrimination with some recent evidence from the olfactory organ. Br. Med. Bull. 6, 330–333.
Aiello, L.C., Wheeler, P, 1995. The expensive-tissue hypothesis: the brain and the digestive system in human and primate evolution. Curr. Anthropol. 36, 199–221.
Bhandawat, V., Olsen, S.R., Gouwens, N.W., Schlief, M.L., Wilson, R.W., 2007. Sensory processing in the Drosophila antennal lobe increases reliability and separability of ensemble odor representations. Nat. Neurosci. 10, 1474–1482.
Barlow, H.B., 1969. Trigger features, adaptation and economy of impulses. In: Leibovic, K.N. (Ed.), Information Processing in the Nervous System. Springer-Verlag, New York, pp. 209–226.
Byrd, C.A., Burd, G.D., 1991. Development of the olfactory bulb in the clawed frog, *Xenopus laevis*. A morphological and quantitative analysis. J. Comp. Neurol. 314, 79–90.
Carey, R.M., Verhagen, J.V., Wesson, D.W., Pírez, N., Wachowiak, M., 2009. Temporal structure of receptor neuron input to the olfactory bulb imaged in behaving rats. J. Neurophysiol. 101, 1073–1088.
Chaput, M.A., El Mountassir, F., Atanasova, B., Thomas-Danguin, T., Le Bon, A.M., Perrut, A., Ferry, B., Duchamp-Viret, P., 2012. Interactions of odorants with olfactory receptors and receptor neurons match the perceptual dynamics observed for woody and fruity odorant mixtures. Eur. J. Neurosci. 35, 584–597.
de Bruyne, M, Foster, K, Carlson, JR, 2001. Odor coding in the Drosophila antenna. Neuron 30, 537–552.
Duchamp, A., Sicard, G., 1984. Influence of stimulus intensity on odour discrimination by olfactory bulb neurons as compared with receptor cells. Chem. Senses 8, 355–366.
Duchamp, A., Revial, M.F., Holley, A., MacLeod, P., 1974. Odor discrimination by frog olfactory receptors. Chem. Senses 1, 213–233.
Duchamp-Viret, P., Chaput, M.A., Duchamp, A., 1989. Amplifying role of convergence in olfactory system. A comparative study of receptor cell and second order neuron sensitivities. J. Neurophysiol. 61, 1085–1094.
Duchamp-Viret, P., Duchamp, A., Vigouroux, M., 1990. Temporal aspects of information processing in the first two stages of the frog olfactory system: influence of stimulus intensity. Chem. Senses 15, 349–365.
Duchamp-Viret, P., Duchamp, A., 1997. Odor processing in the frog olfactory system. Prog. Neurobiol. 53, 561–602.
Duchamp-Viret, P., Duchamp, A., Chaput, M.A., 2003. A. Single olfactory sensory neurons simultaneously integrate the components of an odor mixture. Eur. J. Neurosci. 18, 2690–2696.
Fletcher, M.L., Masurkar, A.V., Xing, J., Imamura, F., Xiong, W., Nagayama, S., Mutoh, H., Greer, C.A., Knöpfel, T., Chen, W.R., 2009. Optical imaging of postsynaptic odor representation in

the glomerular layer of the mouse olfactory bulb. J. Neurophysiol. 102, 817–830.
Friedrich, R.W., Stopfer, M., 2001. Recent dynamics in olfactory population coding. Curr. Opi. Neurobiol. 11, 468–474.
Gesteland, R.C., Howland, B., Lettvin, J.Y., Pitts, V.H., 1959. Comments on microelectrodes. Proc. Inst. Radio Eng. 47, 1856–1862.
Grosmaître, X., Vassalli, A., Mombaerts, P., Shepherd, G.M., Ma, M., 2006. Odorant responses of olfactory sensory neurons expressing the odorant receptor MOR23: a patch clamp analysis in gene-targeted mice. Proc. Natl. Acad. Sci. USA 103, 1970–1975.
Hildebrand, J.G., Shepherd, G.M., 1997. Mechanisms of olfactory discrimination: converging evidence for common principles across phyla. Annu. Rev. Neurosci. 20, 595–631.
Ito, I., Bazhenov, M., Chik-ying Ong, R., Raman, B., Stopfer, M., 2009. Frequency transitions in odor-evoked neural oscillations. Neuron 64, 692–706.
Jiang, T., Holley, A., 1992. Morphological variations among output neurons of the olfactory bulb in the frog (Rana ridibunda). J. Comp. Neurol. 320, 86–96.
Kass, R.E., Ventura, V., Brown, E.N., 2005. Statistical issues in the analysis of neuronal data. J. Neurophysiol. 94, 8–25.
Kostal, L., Lansky, P., Rospars, J.-P., 2008. Efficient olfactory coding in the pheromone receptor neuron of a moth. PLoS Comput. Biol. 4, e1000053, http://dx.doi.org/10.1371/journal.pcbi.10000053.
Laughlin, S.B., 1981. A simple coding procedure enhances a neuron's information capacity. Z. Naturforsch. 36, 910–912.
Laurent, G., 2002. Olfactory network dynamics and the coding of multidimensional signals. Nat. Rev. Neurosci. 3, 884–895.
Lennie, P., 2003. The cost of cortical computation. Curr. Biol. 13, 493–497.
Levy, W.B., Baxter, R.A., 1996. Energy efficient neural codes. Neural Comput. 8, 531–543.
Lledo, J-M., Lagier, S., 2006. Adjusting neurophysiological computations in the adult olfactory bulb. Semin. Cell Dev. Biol. 17, 443–453.
Mazor, O., Laurent, G., 2005. Transient dynamics versus fixed points in odor representations by locust antennal lobe projection neurons. Neuron 48, 661–673.
Münch, D., Schmeichel, B., Silbering, A.F., Galizia, C.G., 2013. Weaker ligands can dominate an odor blend due to syntopic interactions. Chem. Senseshttp://dxdoi.org/10.1093/chemse/bjs138.
Namiki, S., Kanzaki, R., 2011. Offset response of the olfactory projection neurons in the moth antennal lobe. BioSystems 103, 348–354.
Nawrot, M., Aertsen, A., Rotter, S., 1999. Single-trial estimation of neuronal firing rates: from single-neuron spike trains to population activity. J. Neurosci. Methods 94, 81–92.
Nawroth, J.C., Greer, C.A., Chen, W.R., Laughlin, S.B., Shepherd, G. M., 2007. An energy budget for the olfactory glomerulus. J. Neurosci. Methods 27, 9790–9800.
Niessing, J., Friedrich, R.W., 2010. Olfactory pattern classification by discrete neuronal network states. Nature 465, 47–52.
Niven, J.E., Laughlin, S.B., 2008. Energy limitation as a selective pressure on the evolution of sensory systems. J. Exp. Biol. 211, 1792–1804.
Northcutt, R.G., Royce, G.J., 1975. Olfactory bulb projections in the bullfrog Rana catesbeiana. J. Morphol. 145, 251–268.
Oka, Y., Katada, S., Omura, M., Suwa, M., Yoshihara, Y., Touhara, K., 2006. Odorant receptor map in the mouse olfactory bulb: in vivo sensitivity and specificity of receptor-defined glomeruli. Neuron 52, 857–869.
Olshausen, B.A., Field, D.J., 2004. Sparse coding of sensory inputs. Curr. Opin. Neurobiol. 14, 481–487.
Pouget, A., Dayan, P., Zemel, R.S., 2003. Inferences and computation with population codes. Annu. Rev Neurosci. 26, 381–410.
Revial, M.F., Sicard, G., Duchamp, A., Holley, A., 1983. New studies on odor discrimination in the frog's olfactory receptor cells. 1. Experimental results. Chem. Senses 25, 293–311.
Richmond, B.J., Optican, L.M., Spitzer, H., 1990. Temporal encoding of two-dimensional patterns by single units in primate primary visual cortex: I: stimulus-response relations. J. Neurophysiol. 64, 351–369.
Rospars, J.P., 1988. Structure and development of the insect antennodeutocerebral system. Int. J. Insect Morphol. Embryol. 17, 243–294.
Rospars, J.P., Fort, J.C., 1994. Coding of odor quality: roles of convergence and inhibition. Network: Comput. Neural Syst. 5, 121–145.
Rospars, J.P., Lansky, P., Vaillant, J., Duchamp-Viret, P., Duchamp, A., 1994. Spontaneous activity of first- and second-order neurons in the olfactory system. Brain Res. 662, 31–44.
Rospars, J.P., Lansky, P., Duchamp-Viret, P., Duchamp, A., 2003. Relation between stimulus and response in frog olfactory receptor neurons in vivo. Eur. J. Neurosci. 18, 1135–1154.
Rospars, J.-P., Lansky, P., Chaput, M., Duchamp-Viret, P., 2008. Competitive and noncompetitive odorant interactions in the early neural coding of odorant mixtures. J. Neurosci. 28, 2659–2666.
Sandström, M., Lansner, A., Hellgren-Kotaleski, J., Rospars, J.-P., 2009. Modelling the population of olfactory receptor neurons. J. Comput. Neurosci. 27, 337–355.
Sanderson, AC, 1980. Adaptive filtering of neuronal spike train data. IEEE Trans. Biomed. Eng. 27, 271–274.
Scalia, F., 1976. Structure of the olfactory and accessory system. In: Llinas, R., Precht, W. (Eds.), Frog Neurobiology. Springer, Berlin, Heidelberg, New York, pp. 213–233.
Shepherd, G.M., Chen, W.R., Greer, C., 2004. Olfactory bulb. In: Shepherd, G.M. (Ed.), The Synaptic Organization of the Brain. Oxford UP, New York, pp. 165–216.
Sicard, G., Holley, A., 1984. Receptor cell responses to odorant: similarities and differences among odorants. Brain Res. 292, 283–296.
Simoncelli, E.P., Olshausen, B.A., 2001. Natural image statistics and neural representation. Annu. Rev. Neurosci. 24, 1193–1216.
Sokoloff, L., 1989. Circulation and energy metabolism of the brain. In: Siegel, G.F., Agranoff, B.W., Albers, R.W., Molinoff, P.B. (Eds.), Basic Neurochemistry: Molecular, Cellular, and Medical Aspects 4th Edition Raven Press, New York, pp. 565–590.
Stopfer, M., Jayaraman, V., Laurent, G., 2003. Intensity versus identity coding in an olfactory system. Neuron 39, 991–1004.
Szücs, A., 1998. Applications of the spike density function in analysis of neuronal firing patterns. J. Neurosci. Methods 81, 159–167.
Van Drongelen, W., Holley, A., Døving, K.B., 1978. Convergence in the olfactory system: quantitative aspects of odour sensitivity. J. Theor. Biol. 71, 39–48.
Vigouroux, M., Viret, P., Duchamp, A., 1988. A wide concentration range olfactometer for delivery of short reproducible odor pulses. J. Neurosci. Methods 24, 57–63.
Wilson, R.I., Mainen, Z.F., 2006. Early events in olfactory processing. Annu. Rev. Neurosci. 29, 163–201.